The Occurrence of Single Hard X-Ray Sources in Solar Flares

C. P. Goff[1], S. A. Matthews, and L. K. Harra

[1] *Mullard Space Science Laboratory, Holmbury St. Mary, Dorking, Surrey RH5 6NT,United Kingdom.*

ABSTRACT

The 'standard' thick target flare model predicts the existence of strong hard X-ray emission at the footpoints of a flare loop. However, Yohkoh observations suggest that up to 20% of events with data available in three or more Hard X-ray Telescope (HXT) channels show only a single source. Combining datasets from Yohkoh, the Solar and Heliospheric Observatory (SOHO), and Nobeyama Radio Heliograph (NoRH), we compare the characteristics of these single source events to double source events. The objective of this study is to determine whether these represent unresolved double footpoints, asymmetric electron deposition due to magnetic mirroring effects, or a genuine departure from the 'standard' model.

INTRODUCTION

The two-ribbon structure in solar flares is well known and many theoretical models have been proposed to explain the observations, e.g., Sturrock (1966) and Kopp and Pneuman (1976). More recently Shibata et al. (1995) proposed a 'unified' flare model, where reconnection above a flare loop accelerates non-thermal electrons along field lines to the chromosphere. Here they interact with ambient protons and electrons, producing an array of observable signatures. In particular, hard X-rays at the flare footpoints either side of a magnetic neutral line are predicted, which move apart as reconnection progresses. Additionally a loop-top source has been observed (Masuda, 1994) in a number of limb events, where it is possible to detect low intensity emission.

An alternate model is the interacting loop model (e.g. Hanaoka 1996). When magnetic flux emerges from beneath a larger magnetic loop, the orientation can be such that the conditions for reconnection are met. This interaction gives rise to a three legged structure. This model expects two hard X-ray (HXR) footpoints in Yohkoh data over the magnetically bipolar region. Hard X-rays are not observed at the remote site as the electrons responsible are often trapped in the main region and those that are not have a long distance to travel resulting in weak emission that is outside of the dynamic range of HXT.

It has been observed that there is often an asymmetry in the brightness of the footpoints during the impulsive phase (Sakao, 1994). When compared to photospheric magnetic fields the brighter HXR source is normally located in the weaker magnetic field region. In the stronger magnetic field region convergence is higher and thus electron precipitation is reduced due to magnetic mirroring effects. It is possible to measure the magnetic flux density at the loop footpoints with data from the Michelson Doppler Imager (MDI; Scherrer et al. 1995) and compare the field at each, assuming a filling factor of unity. Thus one would expect that the higher the ratio between the footpoint field strengths the greater the difference in intensity between the emission of hard X-rays. However, Asai et al. (2002) found this not to be the case for a flare of April 10th 2001. It was found that the photospheric field strengths at the $H\alpha$ kernels with HXR sources were 3 times higher than those at the $H\alpha$ kernels without HXR sources in this particular event. An estimation of the energy release rate in each kernel found that the $H\alpha$ sources with HXR had a much

higher rate than the others, possibly accounting for the differing appearance.

Since the double HXR footpoint scenario is not always observed, this study investigates the nature of single hard X-ray source events. Although up to 20% of events with data in three or more HXT channels exhibit single source behavior, half of these are very close to the limb or do not have supporting data. Ten flares were chosen due to their single source nature and position on the disk, as recorded by Yohkoh. This paper concentrates on a single event, 2nd May 1998, but summarises the results of all ten.

OBSERVATIONS AND ANALYSIS

We use data from the following sources to study this phenomenon: (1) Yohkoh Soft X-Ray Telescope, which images soft X-rays (SXR) through a grazing incidence telescope and 4 filters covering the energy range 0.25-4 keV(SXT; Tsuneta et al. 1991); (2) HXT (Kosugi et al. 1991) on Yohkoh for observations of 10 - 100 keV hard X-rays from non-thermal electrons and super-hot plasmas in 4 discrete energy channels (L: 14-23 keV, M1: 23-33 keV, M2: 33-53 keV and H: 53-93 keV); (3) Imaging data at 17 GHz from NoRH (Nishio et al. 1994) and (4) longitudinal magnetograms from MDI (Scherrer et al. 1995) on SOHO.

This study covers 10 events showing single HXR source emission, in images reconstructed using the maximum entropy method (MEM), which were directly compared to 11 events with double source structure. All events had hard X-ray data in at least three of the four HXT channels and occurred away from the limb to minimize line of sight influences and to be sure that a second source was not obscured. The bulk properties of each flare are tabulated in Tables 1 & 2.

The tables below list the SXR areas and HXR intensity contained within a 20% brightness contour of the image. This is within the ratio of the lowest reliable contour level with respect to the peak (Sato et al, 1999). Most of the HXR single sources are small and may simply be compact with any structure beyond the resolution of HXT, athough there is often elongation of these sources with time. The soft X-ray images and radio emission, in the 2nd May 1998 event (detailed later), suggest a loop-loop interaction, although unlike Hanaoka events there is only a single HXR source. This may be due to the specific geometry of this flare or it may simply be that the other HXR source is very faint and is not observed due to the dynamic range of HXT. It should, however, be noted that the MEM procedure can over resolve images, although steps have been taken to improve the MEM formulation (Sato, et al, 1999) with the inclusion of the total flux estimate. Work has also begun in the reconstruction of the HXR images using the Pixon method, with its improved photometry.

Table 1. Bulk Properties of Single HXR Source Events: where SXR_A is the area of the SXR loop, HXR_L and HXR_{M2} are the HXR brightness in L and M2 channels respectively, F_{HXR} and F_{Foot} are the average magnetic flux densities at the HXR footpoint and other footpoint respectively, γ and is the spectral index at the maximum assuming a single power law

Date	SXR_A $arcsec^2$	HXR_L $counts/s$	HXR_{M2} $counts/s$	F_{HXR} (G)	F_{Foot} (G)	γ
2-Apr-2001	589	337	4	201	-290	6.3
5-Mar-2000	127	5	2	121	-205	2.4
27-Mar-2000	253	13	5	-116	151	3.6
1-Feb-2001	259	19	1	125	-300	3.6
10-Mar-2001	149	1225	30	110	-174	2.4
25-Aug-1999	198	80	2	-212	258	3.2
23-Jun-2001	165	1561	34	-319	423	6.8
20-Sep-2001	127	14	2	169	-264	3.2
31-Mar-2000	160	19	1	-201	219	4.0
02-May-1998	578	4	4	295	-324	2.4
Mean Magnitudes	261	328	9	187	261	3.8

In addition, the spectral index evolution was studied and the index at the peak of the hard X-ray emission is quoted in the summary tables (γ). To allow direct comparison a single power law was fitted to data from

Table 2. Bulk Properties Of Double HXR Source Event: the headings are as in Table 1 except HXR_{LB} and HXR_{M2B} are the brightness of the brighter footpoint and HXR_{LD} and HXR_{M2D} of the darker, F_{HXR} is the mean magnetic flux under the strong HXR source and F_{Foot} is the average flux under the weaker HXR footpoint.

Date	SXR_A $arcsec^2$	HXR_{LB} $counts/s$	HXR_{LD} $counts/s$	HXR_{M2B} $counts/s$	HXR_{M2D} $counts/s$	F_{HXR} (G)	F_{Foot} (G)	γ
15-Nov-1991	330	396	160	78	10	100	-400	3.1
3-Dec-1991	220	1592	277	115	77	-80	300	4.0
7-Feb-1992	270	19	2	5	1	-30	200	3.4
2-Nov-1991	451	128	56	43	23	-100	400	3.4
2-Oct-1993	165	5	3	1	1	300	-780	3.9
6-Nov-1997	160	1115	143	952	875	-200	554	2.3
6-Sep-1998	336	5	1	2	1	-320	751	3.1
25-Aug-2001	506	1442	524	473	105	401	-601	3.2
31-Aug-2001	292	17	10	9	3	-154	325	1.9
10-Sep-2001	182	7	6	1	1	-150	358	4.0
07-Sep-2001	858	14	1	6	1	-461	670	4.1
Mean Magnitudes	343	431	108	153	100	209	485	3.3

the L, M1 and M2 channels, which proved to be a good representation of the events. Nearly all of the events studied followed the soft-hard-soft pattern in their evolution, first recognised by Parks and Winkler (1969), with the exception of 3 events which followed a hard-soft pattern. Also in each case there is a range of values all between 1.9 and 4.1, with the exception of two events with single sources, which are much softer. Again there is no distinct difference between the two sets of data.

Magnetic Field

To assess the effects of magnetic asymmetry in events it is necessary to find the magnetic field at each of the flare footpoints. In order to do this HXT image contours were overlaid on MDI images, the magnetograms were differentially rotated to the time of the event and the data were corrected for line of sight effects due to disk position to give better estimations of the field. The flux densities for each MDI pixel within a 40% HXT contour at each footpoint were averaged. In addition, the pixels within a 20% contour (lowest confidence level) were averaged and the difference between these values was used as the uncertainty in the measurement, represented graphically as the error bars in Figure 1.

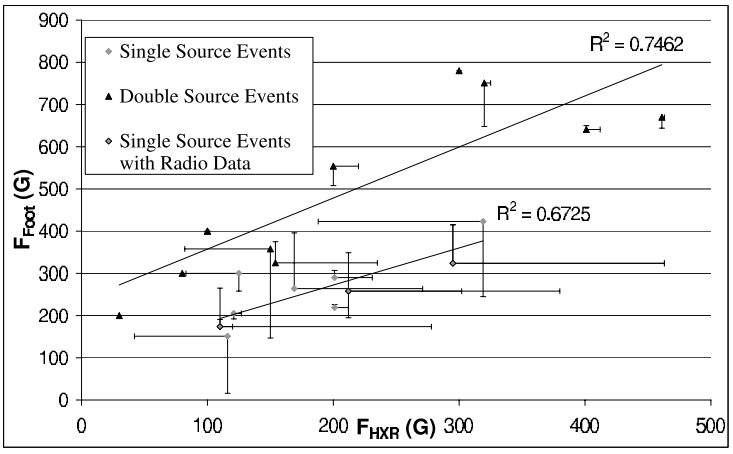

Fig. 1. Plot of average flux densities (Listed in Tables 1 and 2) at each footpoint of the flaring loops where R^2 is the correlation coefficient

In the case of single HXR source flares the second footpoint is estimated using the SXT image and magnetogram as boundary positions. The small SXR source is generally found across the magnetic neutral line and is typically offset from the HXR source. The single HXR source is also found at this neutral line, but is centred to one side. With three of the sample we were fortunate to have radio imaging data

from Nobeyama. These images are constructed by application of the Hanaoka procedure which applies the CLEAN principle. In these cases the total intensity 17 GHz images were used to refine the position of the second footpoint. Contours were again used to constrain the area of interest and the average flux densities determined. Although radio emission is generally formed higher in the corona and is not on its own a good representation of a flare footpoint, it provides additional insight into these compact events. The co-alignment of these images is better than 5". In addition it was necessary to assume that the loop was symmetrical and thus the estimated areas used were equal to that of the HXR footpoint. In future work it is hoped that we can improve on these results by using the distribution of footpoint size differences, in the double source cases, to get a more realistic estimate of the unseen footpoint in the single source events.

When using MDI data it is important to be aware of the limitations. The MDI data itself is a measure of the longitudinal magnetic flux at the photosphere and corrections made make the assumption that the field is radial at the photosphere. This may be the case in the very strong field toward the centre of the sunspot, but at the edges, where it is likely flares occur, it is more realistic that the field lines will have some other orientation. This cannot be corrected for as the fields measured are only the longitudinal portion of the total field and the orientation of the field at the point of the flare is unknown, which leads to an underestimation of the field. The combined pointing accuracy of HXT and MDI is of the order of 1 MDI pixel which is also a source of error, especially in regions of widely varying flux.

The longitudinal magnetic field data for both samples are plotted in Figure 1 where, F_{HXR} represents the flux density of the single HXR source in addition to the strong HXR source in the double source event, and F_{Foot} represents the flux density of the estimated invisible HXR footpoint in the single source events along with the weaker source in the double footpoint events. It is apparent that the slope of single source event data is shallower than that associated with the double source events suggesting that the asymmetry may actually be less. However, MDI measurements are only the longitudinal field and the mirror ratio depends on the total magnetic field. In addition the uncertainties in this work are large. It may be that the distinction is skewed by the measuring method and that they are in fact the same population as the double sources, or alternatively one of the other uncertainties may be more influential in the single source events than the double.

To illustrate the points above more clearly the 2nd May 1998 event is focused on below.

2nd May 1998

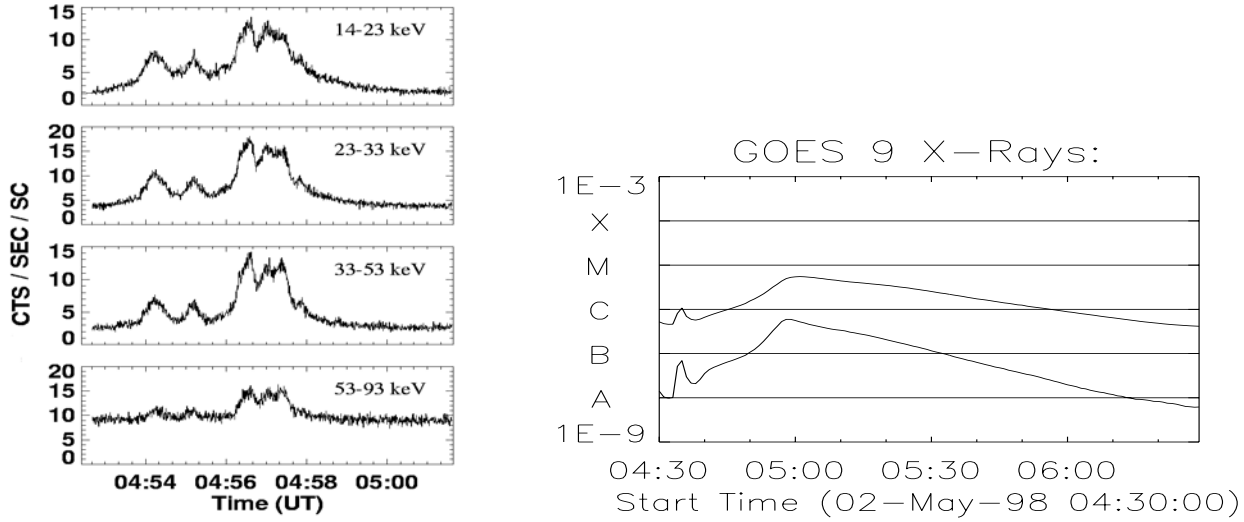

Fig. 2. Left: HXT light curves over all 4 channels showing the impulsive behavior over 4 minutes Right: GOES light curve of the same event, showing the gradual rise and decline of the thermal SXR emission

This flare occurred in active region 8210 at approximately 04:53 UT. The flare was recorded by SXT, HXT, MDI and NoRH. X-ray light curves from all four HXT channels and from GOES can be seen in Figure 2. Figure 3 presents full resolution soft X-ray images of this event in Be119 filter and shows the evolution of this thermal emission. The central image in Figure 3 represents SXR at the peak of emission. The first

image is from the early part of the impulsive phase and the third from the decay phase of the event. The emission was dominated by a single loop structure for the first 18 minutes of the flare period. As the flare reaches the end of its life two distinct SXR patches form for the remaining 5 minutes of the observation.

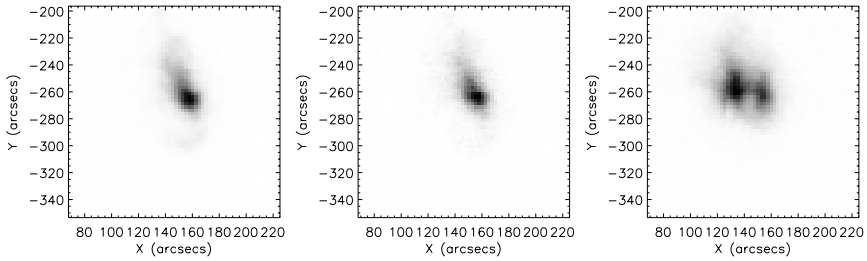

Fig. 3. Evolution of SXT images over the flare time. The first image was during the rise phase (04:54:23 UT), the second was at the peak (04:56:37 UT) and the third was during the decay phase (05:08:57 UT)

Using data from HXT it was possible to reconstruct images of the HXR emission using the maximum entropy method (MEM; Gull and Daniell, 1978). Figure. 4 illustrates the relation of the HXR images in the M2 channel to the SXR loop and how the positioning of the HXR source changes with time. As time progressed the HXR source gradually moved from west to east by 5 arc seconds.

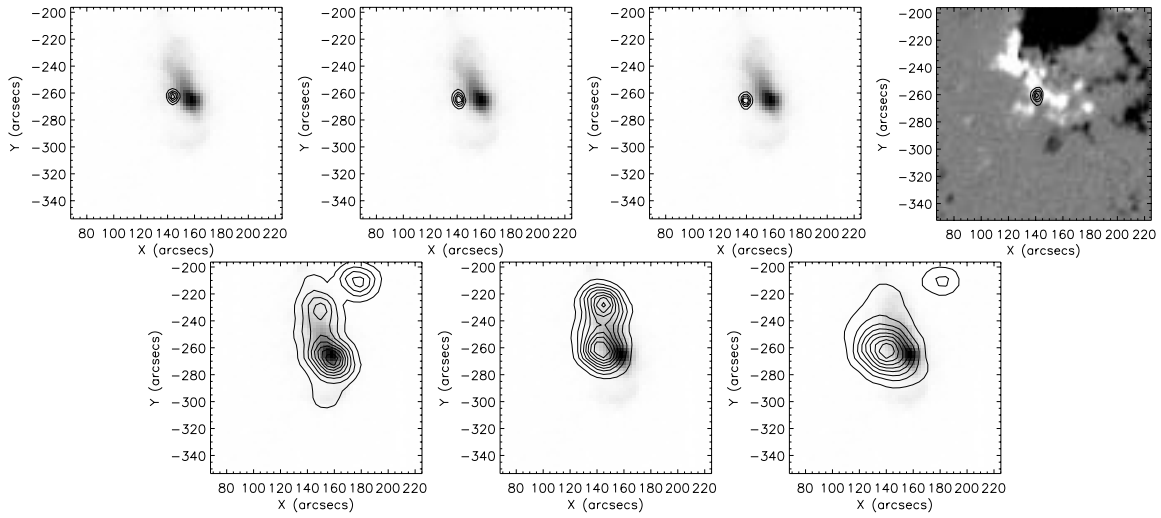

Fig. 4. Top: The first three greyscale image show SXR (04:54:23) and on these are HXR contours at 04:55:11, 04:56:44 and 04:57:30 UT respectively. The fourth images is a magnetogram from MDI differentially rotated to the time of the flare (04:54 UT) and overlaid with HXR contours at 04:56:44 UT. Bottom: The first three are the same greyscale image as above but are overlaid with 17Ghz radio contours at 04:53:24, 04:56:25 and 05:21:12 UT.

Shown in the lower panels of Figure 4 are total intensity image contours of 17GHz radio emission from Nobeyama, thought to be produced by gyro-synchrotron emission. Again the evolution of the images with time is apparent. At 04:53 the images appear to show three footpoints. However, the north-west source, in the first image, does not appear to correspond directly to the soft X-ray loop. After a few minutes, at 04:56, there are only two sources. The northern source remains fixed in both images but the southern most sources moves north-east. This source is coincident with the HXR source previously mentioned. This is illustrated best in the centre images in Figure 4 where the times of occurrence are very similar. This radio source is present throughout the time of the HXR source.

The addition of the radio sources and the changing morphology of the SXT image suggest that there may be two interacting loops in this flare event. One loop is clearly seen in soft X-ray and the other is best recognised by the footpoint radio emission. When we relate this back to Figure 3 the last image may be the result of reconnection between two loops rooted by the radio footpoints.

The HXT image contours were overlaid on an MDI image Figure 4. In this case the flux density under the HXR footpoint was found to be around 295 G and at the end of the loop where only radio was observed at -324 G.

DISCUSSION AND CONCLUSIONS

Ten single HXR source and eleven double HXR sources have been examined and a summary table of results can be seen in Tables 1 and 2. A multi-wavelength analysis has been performed on each of the events listed including data in soft X-ray, hard X-ray, radio wavelengths and magnetograms.

The two single source events with the largest SXR areas may be loop-loop interactions, similar to Hanaoka events. However, contrary to Hanaoka findings they do not have two visible HXR sources. It is not known whether there is an additional source below the dynamic range of the HXT instrument or if this is really one source. The remaining events appear to be compact with a small SXR image lying in a region of mixed magnetic polarity across the magnetic inversion line, suggesting the loop is simply unresolved.

It is clear from the results that magnetic mirroring is supported, however there is very little difference between the slopes of the two lines in Figure 1, although this difference is minor compared to the uncertainties involved with the data. This difference could be due to systematic measurement errors, especially in the estimation of the second invisible footpoint in the single HXR source events. In the larger events it is possible that geometry plays a role in addition to mirroring. The geometry of the loop would determine the site of acceleration which would in turn determine the path the electrons take. In addition, the hard X-ray images discussed in this paper are being constructed using the Pixon method. With these results it may be possible to reduce the errors on this work.

In the smaller, more compact events, it is likely that many of these are simply un-resolvable by HXT. The small regions of soft X-ray emission are located in these regions of mixed magnetic polarity and in seven events show an elongation with time. For these type of events improvements in spatial resolution and dynamic range from RHESSI may help this study.

REFERENCES

Asai, A., S. Masuda, T. Yokoyama, et al. Difference between spatial distributions of the $H\alpha$ kernels and hard X-ray sources in a solar flare, *ApJ*, *451*, L91-L94, 2002.

Gull,S.F., G. J. Daniell, Image reconstruction from incomplete and noisy data, *Nature*, *272*, 686-690, 1978.

Hanaoka, Y., Flares and plasma flow caused by interacting coronal loops, *Sol. Phys.*, *165*, 275-301, 1996.

Kane, S. R., Impulsive phase of solar flares: hard X-ray, microwave,EUV and optical observations, *Coronal Disturbances* , 105, 1974.

Kopp, R. A., G. W. Pneuman, Magnetic reconnection in the corona and the loop prominence phenomenon, *Sol. Phys.*, *50*, 85-98, 1976.

Kosugi, T., K. Makishima, T. Murakami, The hard X-ray telescope (HXT) for the Solar-A mission, *Sol. Phys.*, *136*, 17-36, 1991.

Masuda, S., Hard X-ray sources and the primary energy release site in solar flares, Ph.D Thesis, University of Tokyo, 1994.

Nishio,M., H. Nakajima, S. Enome, et al. The Nobeyama Radioheliograph, *Kofu Symposium*, 19-33, 1994.

Sakao, T., Characteristics of solar flare hard X-ray sources as revealed with the hard X-ray telescope aboard the Yohkoh satellite, Ph.D Thesis, University of Tokyo, 1994.

Sato, J., T. Kosugi, K. Makishima, Improvement of Yohkoh Hard X-Ray Imaging, *PASJ*, *51*, 127-150, 1999.

Shibata, K., S. Masuda, M. Shimojo, et al., Hot-Plasma ejections associated with compact-loop solar flares, *ApJ*, *451*, L83-L85, 1995.

Scherrer, P. H., R. S. Bogart, R. I. Bush, The solar oscillations investigation - Michelson Doppler Imager, *Sol. Phys.*, *162*, 129-188, 1995.

Sturrock, P. A., Model of high-energy phase of solar flares, *Nature*, *211*, 695-697, 1966.

Tsuneta,S., L. Acton, M. Bruner, The soft X-ray telescope for the Solar-A mission, *Sol. Phys.*, *136*, 37-67, 1991.

Email Address of C. Goff cpg1@mssl.ucl.ac.uk

Manuscript received 30 November, 2002; revised 09 April, 2003; accepted 13 June, 2003